LETTER

doi:10.1038/nature11520

April 2012 intra-oceanic seismicity off Sumatra boosted by the Banda-Aceh megathrust

Matthias Delescluse[1], Nicolas Chamot-Rooke[1], Rodolphe Cattin[2], Luce Fleitout[1], Olga Trubienko[1] & Christophe Vigny[1]

Large earthquakes nucleate at tectonic plate boundaries, and their occurrence within a plate's interior remains rare and poorly documented, especially offshore. The two large earthquakes that struck the northeastern Indian Ocean on 11 April 2012 are an exception: they are the largest strike-slip events reported in historical times[1,2] and triggered large aftershocks worldwide[3]. Yet they occurred within an intra-oceanic setting along the fossil fabric of the extinct Wharton basin, rather than on a discrete plate boundary[4–8]. Here we show that the 11 April 2012 twin earthquakes are part of a continuing boost of the intraplate deformation between India and Australia that followed the Aceh 2004 and Nias 2005 megathrust earthquakes, subsequent to a stress transfer process recognized at other subduction zones[9,10]. Using Coulomb stress change calculations, we show that the coseismic slips of the Aceh and Nias earthquakes can promote oceanic left-lateral strike-slip earthquakes on pre-existing meridian-aligned fault planes. We further show that persistent viscous relaxation in the asthenospheric mantle several years after the Aceh megathrust explains the time lag between the 2004 megathrust and the 2012 intraplate events. On a short timescale, the 2012 events provide new evidence for the interplay between megathrusts at the subduction interface and intraplate deformation offshore. On a longer geological timescale, the Australian plate, driven by slab-pull forces at the Sunda trench, is detaching from the Indian plate, which is subjected to resisting forces at the Himalayan front[6,8,11].

The first and largest shock of 11 April 2012 (moment magnitude M_w 8.6) occurred 330 km west-southwest of the Aceh 2004 epicentre, but only 120 km southwest of the subduction front. It was followed 2 h later on the same day by an M_w 8.2 twin earthquake, located some 180 km south of the main event. The oceanic fabric there is characterized by a set of more or less north–south-oriented fracture zones, well captured by satellite-derived gravity measurements (Fig. 1) and mapped *in situ* using multi-beam bathymetry[4]. These are fossil transform faults that were active during the opening of the Wharton basin that shut off some 45 Myr ago. Recent reactivation of these faults[12] was confirmed by seismic reflection profiling showing basement and sediment offsets as well as sea-floor expression[13]. The epicentres of the two 11 April 2012 events align along a 022° direction, which is within a few degrees of one of the nodal planes for both earthquakes.

The two twin shocks thus seem to have involved slip on one of these very long fossil fracture zones that can be followed for several hundred kilometres[6]. The perpendicular normal fault orientation only offers limited continuous fault length to the rupture as it is offset by fracture zones[14]. However, we cannot rule out slip on the conjugate plane[15] as such slip happened further south in the Wharton basin in the year 2000[7]. For the M_w 8.6 event, aftershocks (Fig. 1) and back-projection analysis indicate the activation of N110°E planes[16,17]. The entire oceanic fabric, normal faults included, seems to be somewhat reactivated by these complex events.

The 11 April 2012 earthquake sequence is located in an area previously recognized as part of the diffuse deformation zone between the Indian and Australian plates[18]. Intraplate deformation is active on

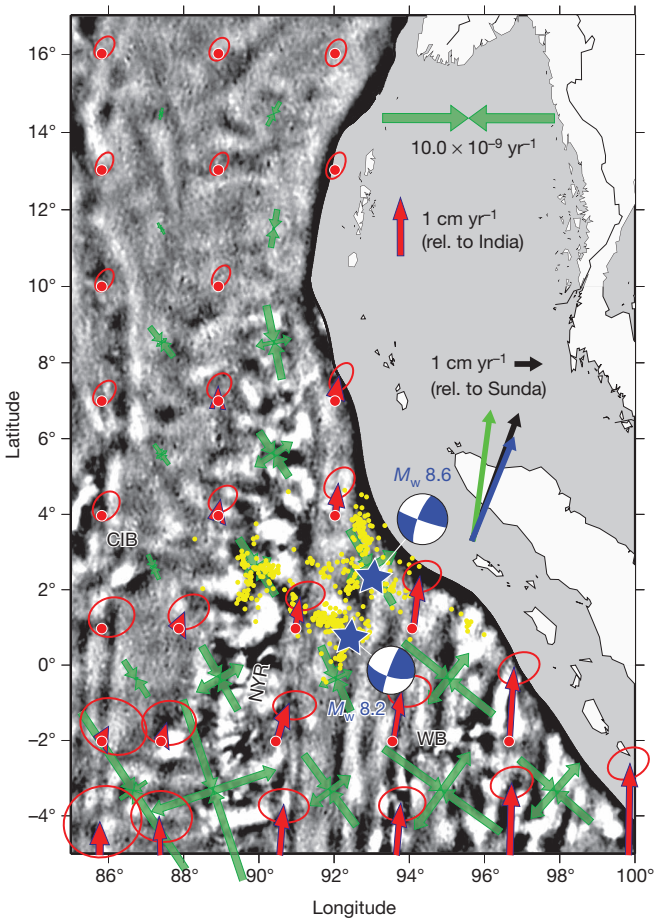

Figure 1 | Present-day kinematics of the India–Australia plate. The 11 April 2012 M_w 8.6 and M_w 8.2 earthquakes, shown here by their blue and white focal mechanisms ('beachballs'), occurred in the Wharton basin (WB), at the heart of the diffuse plate boundary between India and Australia. Ninetyeast Ridge (NYR), which is the Kerguelen hotspot trail, separates the Wharton basin from the central Indian basin (CIB). Off trench, the background is the 120 km high-pass-filtered satellite free-air gravity anomaly, illuminating meridian aligned fracture zones. Three convergence vectors are displayed east of the Sumatra-Andaman trench, calculated at the location of the 2004 Aceh epicentre. The blue vector is India/Sunda vector (IN/SU) predicted by the MORVEL[33] global model (46 mm yr^{-1} towards N22°E), while the green vector is the Australia/Sunda prediction using the same model (54 mm yr^{-1} towards N8°E). The true convergence vector is in between, since the subducting plate is neither India nor Australia. The black vector (56 mm yr^{-1} towards N20°E) is an estimation of the convergence rate that takes into account a non-rigid India-Australia plate. This non-rigid crustal velocity field is shown as red vectors with their 95% error ellipses at knot points west of the trench line. The corresponding strain-rate field is shown as green double arrows. At the latitude of the April 2012 earthquake sequence, motion of the Wharton basin with respect to India progressively increases west to east, from negligible close to Ninetyeast ridge to 10 mm yr^{-1} close to the trench.

[1]Laboratoire de Géologie, Ecole Normale Supérieure and CNRS UMR8538, 75005 Paris, France. [2]Géosciences Montpellier, Université Montpellier II and CNRS UMR5243, 34090 Montpellier, France.

both sides of Ninetyeast Ridge, predominantly as reverse faults with north–south compressive axes (P-axes) west of it[19–21] and strike-slip faults with northwest–southeast P-axes east of it[4,8]. Large-scale folding of the oceanic lithosphere was found both in the equatorial Indian Ocean and in the Wharton basin, and interpreted as a direct consequence of large in-plate stresses[11]. The present-day kinematics of the Indian and Australian plates is now well established, based on Global Positioning System (GPS) measurement away from the deforming zone. Following the approach of Holt and Haines[5,22] (Methods), we have derived a self-consistent non-rigid velocity field[8] (Fig. 1) that combines far-field boundary conditions (GPS over Australia and India, plus a few islands within the deforming zone) and local constraints from the deformation zone itself (style of deformation from focal mechanisms and heat flow as a proxy for strength). Offshore from Sumatra, the motion exhibits a gradual south–north evolution from the Australian plate velocity to the Indian plate velocity. The predicted amount of shear across the set of meridian aligned faults is of the order of 10 mm yr^{-1}.

Intraplate seismicity has been boosted by the Aceh and Nias ruptures. We show in Fig. 2 a chrono-spatial chart of the seismicity of the Wharton basin, covering the 8 years before and the 8 years after the Aceh earthquake. An increase in the rate of seismicity immediately followed the Aceh and Nias earthquakes, especially for the portions of oceanic lithosphere experiencing peak slip rate on the failure plane of the Aceh megathrust. The Nias earthquake that followed the Aceh earthquake triggered oceanic earthquakes in a region that remained silent during the time lag of three months between the two events. We also estimated the net increase in intraplate seismic moment release. On the basis of a century-long catalogue[8], the mean moment release for the entire deforming Indian Ocean (including the central Indian basin and the Wharton basin) was about 2.3×10^{19} N m yr^{-1} before the Aceh earthquake, two-thirds of it being released in the Wharton basin. In the year 2005, this number jumped to 1.2×10^{20} N m for the Wharton basin only. For comparison, seismic moment release for the two 11 April earthquakes is above 1.4×10^{22} N m, which is about 1,000 times the yearly release estimated from the century-long catalogue.

We compiled focal mechanisms of 47 earthquakes ($M_w > 5$) that occurred off Sumatra in the oceanic plate from December 2004 (Aceh earthquake) until 15 April 2012 (from the Global CMT catalogue). We excluded earthquakes within the slab portions already engaged in subduction, although many of them are clearly related to intraplate deformation and reactivation of the oceanic fabric[7], such as the Padang earthquake of 2009 (M_w 7.6, depth >80 km). The post-Aceh oceanic earthquakes fall into two categories: normal faults at the external wall of the trench (18 events), and earthquakes with a northwest–southeast P-axis corresponding to the release of India-Australia intraplate stress (29 earthquakes). Among the compressive events, only one seems unrelated to the oceanic fabric, the other 28 being strike-slip earthquakes with one left-lateral meridian aligned nodal plane (015° ± 005°). The very consistent orientation of the nodal planes over a wide region is strong evidence for reactivation of the oceanic fabric in the area.

To test the effect of the Aceh 2004 and Nias 2005 ruptures on the reactivation of the Wharton basin oceanic fabric, we calculated the far-field static Coulomb stress change $\Delta CFF = \Delta\tau - \mu'\Delta\sigma_n$ resulting from the coseismic displacement on the subduction interface, up to 250 km seaward of the trench axis. Here $\Delta\tau$ is the static shear stress change on the failure planes (positive in the direction of fault slip), $\Delta\sigma_n$ the static normal stress change (positive if the fault is clamped) and μ' the effective friction coefficient (see Methods and ref. 23). A positive Coulomb stress change favours rupture.

Calculations were first performed to resolve stress onto a N15°E-oriented vertical plane (Fig. 3a). The Coulomb stress change is calculated at 18 km depth, which is the average depth of the earthquakes before 2012 and an upper limit for the centroid depth of the mainshock of 11 April 2012 (18–27 km; ref. 14). We find that all strike-slip earthquakes occurred in a lobe of positive Coulomb stress change. The area of highest Coulomb stress change in front of the 2004 Aceh coseismic

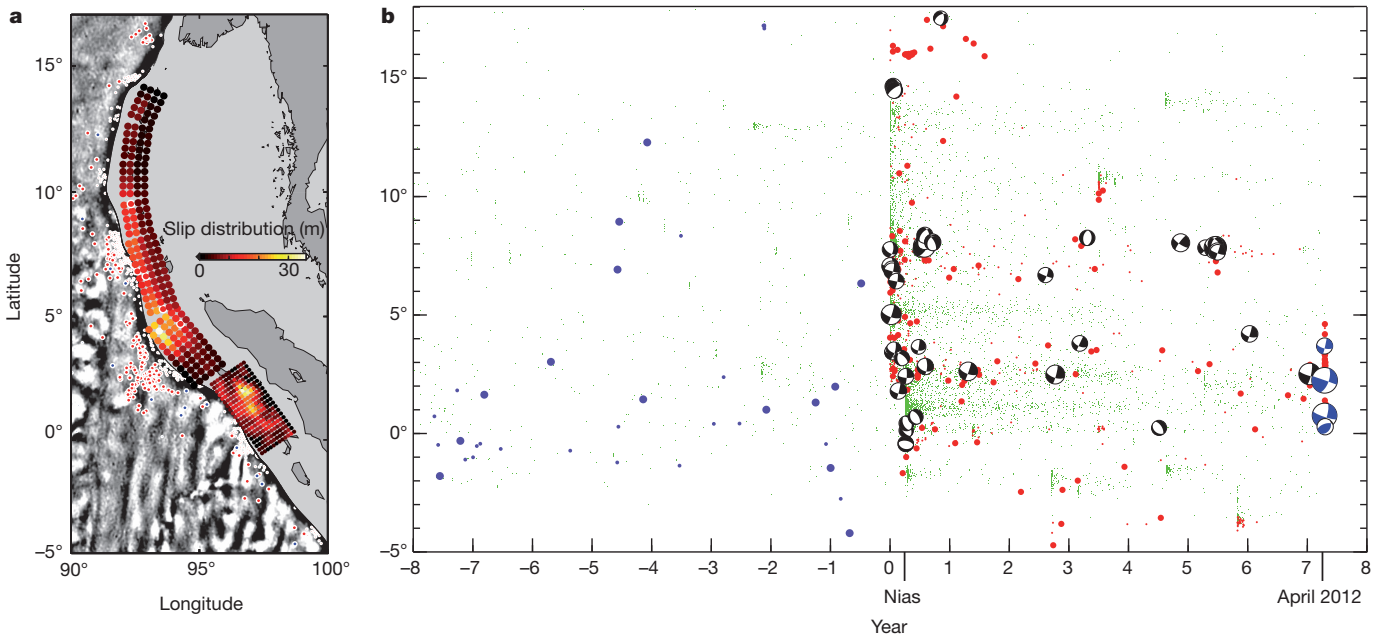

Figure 2 | Oceanic intraplate seismicity boost after the Aceh (2004) and Nias (2005) earthquakes. **a**, Map representation; **b**, chronological chart. **a**, Map representation of the same intraplate seismicity as **b**. To ensure the intraplate nature of the earthquakes, events 50 km off-trench are shown as larger dots. **b**, Year 0 corresponds to 26 December 2004. Red (after December 2004) and blue (before December 2004) events are exclusively located over the oceanic plate west of the trench line and up to 250 km away from the trench line, whereas green points represent the entire seismicity, including the upper plate. All earthquakes were extracted from the NEIC catalogue. Focal mechanisms of post-Aceh events with magnitudes greater than 5 occurred after December 2004 are also displayed. Blue focal mechanisms correspond to the April 2012 earthquake sequence, and black focal mechanisms to earthquakes that occurred in the same area since the Aceh event.

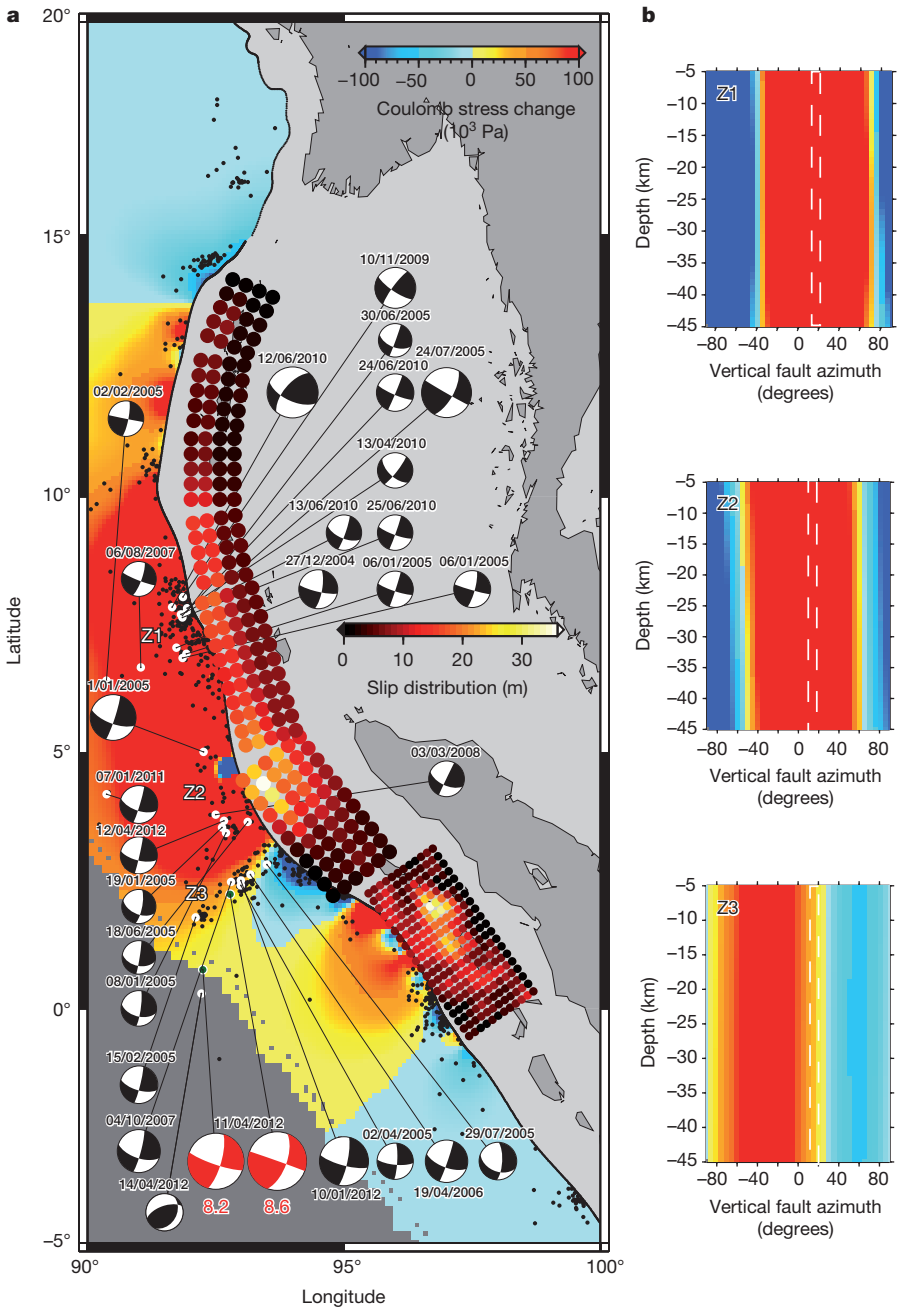

Figure 3 | Static Coulomb stress change calculation offshore the Sumatra-Andaman subduction. **a**, Each colour pixel represents a N15°E-oriented vertical fault plane. Note that the slip colour scale is adapted to the Aceh earthquake slip distribution, and requires division by a factor of three to obtain the Nias earthquake slip values. **b**, The Coulomb stress change has been tested for different depths and azimuths of the fault planes at three different locations, from north to south: Z1 (30 June 2005 earthquake location), Z2 (1 January 2005 earthquake location) and Z3 (11 April 2012 mainshock location). White bars bound the azimuths of the oceanic fabric. Slip on the oceanic fabric is best favoured to the north of the area.

slip corresponds to a shear stress increase and to a normal stress decrease. This situation favours left-lateral strike-slip on the N15°E vertical faults independently of the value of the effective friction coefficient (unclamping). We further tested the effect of the azimuth of the vertical planes and the variation of the Coulomb stress change with depth (Fig. 3b). The mainshock of 11 April 2012 locates the exact limit where N20°E planes are still positively favoured by the Aceh 2004 slip. The Coulomb stress change is much higher if we consider that the M_w 8.6 event nucleated on a N110°E plane with dextral motion (see Supplementary Information), as suggested by seismological studies[16,17]. Depth does not really affect the result for the considered 5–45 km range. The 2005 Nias rupture also favours the occurrence of earthquakes on N15°E-oriented vertical planes, but focal mechanisms there indicate normal rather than strike-slip events. Most of the normal faults oriented along the trench strike are located in areas of positive Coulomb stress change for their respective receiver fault orientation (see Supplementary Information). Slip on newly formed thrust faults perpendicular to the intraplate P-axis are inhibited by the Aceh earthquake coseismic stresses (see Supplementary Information). Over the long term, only a few reverse faults were active during the past century[7], as stresses apparently rarely reached the level required to create a new fault.

The Coulomb stress change distribution is highly sensitive to the coseismic slip distribution. The high sensitivity of the model to shallow slip, in particular, may partly be due to assumptions underlying the Coulomb model, such as a flat-plane subduction interface and an

homogeneous elastic half-space. Many coseismic solutions (see, for example, refs 24–29) have been proposed for the Aceh and Nias earthquakes based on the inversion of various data sets, including GPS displacements, coral reef observations, long-period teleseismic data, tide-gauge records and satellite altimetry measurements. We use here the slip distributions obtained in refs 24 and 25, for the Aceh and Nias earthquakes, respectively. First-order properties of the slip distributions obtained in these two models are consistent with several other studies[26–29]. Our best choice for slip distribution was however driven by one significant observation: triggered intraplate earthquakes, both normal (see Supplementary Information) and strike-slip, occur extremely close to the toe of the trench. Our sensitivity tests showed that only slip distributions including shallow, near trench displacement successfully produce a positive Coulomb stress change close enough to the trench[9]. Most coseismic slip inversions are rather insensitive to shallow displacements at the toe of the subduction, which is generally too far from the land stations where measurements are available. They thus tend to minimize the amount of shallow rupture there. However, marine constraints[30] (2011 Tohoku M_w 9.0 earthquake, Japan), and geodetic measurements close to the failure plane[31] (2010 Maule M_w 8.8 earthquake, Chile) have shown that the coseismic displacement of giant earthquakes does reach the toe of the trench.

A clear drawback of the Coulomb stress calculation is that it fails to model time-dependent stress transfers because the underlying rheology is elastic. In these elastic models, promoted faults should break shortly after the megathrust event, as the extensional stress within the oceanic plate off the trench begins to decrease immediately after the earthquake with the start of a new interseismic loading cycle. Yet the time lag between Aceh and the 2012 earthquake sequence is more than 7 years, which indicates another mechanism producing a northeast–southwest unclamping that is larger than the slow buildup of northeast–southwest compressive stress during interseismic loading. Transient triggering may be related to the viscoelastic properties of the asthenosphere. In Supplementary Information, we present a simple two-dimensional viscoelastic model of the earthquake cycle that predicts the time evolution of the stresses linked to subduction earthquakes as a function of distance to the trench. The observed time lag between the Aceh and Nias earthquakes and the April 2012 earthquake sequence is found to be compatible with a rheology of the asthenosphere independently required to explain near field to far field GPS constraints in the Sunda block, on the other side of the trench[32]. The maximum post-seismic relaxation stress is reached between 7 and 10 years after the megathrust in the area of the 2012 events. The further from the trench, the longer the time lag until maximum post-seismic relaxation stress is reached. Similar three-dimensional finite element viscoelastic calculations[32], using a more realistic rupture zone geometry, further confirm that at the locations of the two events of April 2012, the net stress effect is unclamping in the northeast direction, in agreement with the two-dimensional viscoelastic model and the Coulomb stress change calculations presented here.

The two large earthquakes of 11 April 2012 are typical of the intraplate deformation between the Indian and Australian plates, the fossil fabric of the oceanic lithosphere being re-activated across the entire Indian Ocean[19,21]. The mega-earthquakes of Aceh and Nias acted as instantaneous boosters, suddenly illuminating where and how intraplate deformation was at work. Viscous relaxation in the asthenospheric mantle is responsible for short-term stress building, still contributing several years to several tens of years after the megathrust events. Long-term stress building there[11] is the direct consequence of the high mechanical coupling of the Indian plate to the Eurasian plate at the Himalayan front that started some 8 Myr ago. Dense oceanic slabs engaged at the Sunda trench inexorably drive the Australian plate northward, while this motion is resisted at the Himalayas. The long-term scenario is that a nascent plate tectonic boundary is forming: the Australian plate is becoming detached from the Indian plate.

METHODS SUMMARY

Kinematic modelling. The kinematic model is detailed elsewhere[8]. It includes constraints from far-field GPS measurements and style of deformation from a century-long intraplate earthquake catalogue.

Coulomb stress change calculations. Coseismic stresses are computed using megathrust slip distributions described as displacement discontinuities in an homogeneous elastic half-space[23]. The shear and normal stresses are then extracted for a chosen plane geometry that is supposed to pre-exist in the entire oceanic lithosphere.

Post-seismic relaxation. A two-dimensional finite element model featuring variable rheological parameters is used (Z-set/Zébulon; see Methods). The rheological parameters fit the upper plate GPS constraints.

Full Methods and any associated references are available in the online version of the paper.

Received 30 April; accepted 23 August 2012.
Published online 26 September 2012.

1. Robinson, D. P. A rare great earthquake on an oceanic fossil fracture zone. *Geophys. J. Int.* **186,** 1121–1134 (2011).
2. McGuire, J. J. & Beroza, G. C. A rogue earthquake off Sumatra. *Science* **336,** 1118–1119 (2012).
3. Pollitz, F. F., Stein, R. S., Sevilgen, V. & Bürgmann, R. The 11 April 2012 east Indian Ocean earthquake triggered large aftershocks worldwide. *Nature* http://dx.doi.org/10.1038/nature11504 (this issue).
4. Deplus, C. *et al.* Direct evidence of active deformation in the eastern Indian oceanic plate. *Geology* **26,** 131–134 (1998).
5. Tinnon, M., Holt, W. E. & Haines, A. J. Velocity gradients in the northern Indian Ocean inferred from earthquake moment tensors and relative plate velocities. *J. Geophys. Res.* **100,** 24315–24329 (1995).
6. Deplus, C. Indian Ocean actively deforms. *Science* **292,** 1850–1851 (2001).
7. Abercrombie, R. E., Antolik, M. & Ekstrom, G. The June 2000 Mw 7.9 earthquakes south of Sumatra: deformation in the India-Australia plate. *J. Geophys. Res.* **108,** 2018, http://dx.doi.org/10.1029/2001JB000674 (2003).
8. Delescluse, M. & Chamot-Rooke, N. Instantaneous deformation and kinematics of the India-Australia plate. *Geophys. J. Int.* **168,** 818–842 (2007).
9. Dmowska, R., Rice, J. R., Lovison, L. C. & Josell, D. Stress transfer and seismic phenomena in coupled subduction zones during the earthquake cycle. *J. Geophys. Res.* **93,** 7869–7884 (1988).
10. Lay, T., Ammon, C. J., Kanamori, H., Xue, L. & Kim, M. J. Possible large near-trench slip during the 2011 Mw 9.0 off the Pacific coast Tohoku earthquake. *Earth Planets Space* **63,** 713–718 (2011).
11. Gerbault, M. At what stress level is the central Indian Ocean lithosphere buckling? *Earth Planet. Sci. Lett.* **178,** 165–181 (2000).
12. Rajendran, K., Andrade, V. & Rajendran, C. P. The June 2010 Nicobar earthquake: fault reactivation on the subducting oceanic plate. *Bull. Seismol. Soc. Am.* **101,** 2568–2577 (2011).
13. Graindorge, D. *et al.* Impact of lower plate structure on upper plate deformation at the NW Sumatran convergent margin from seafloor morphology. *Earth Planet. Sci. Lett.* **275,** 201–210 (2008).
14. Satriano, C., Kiraly, E., Bernard, P. & Vilotte, J. P. The 2012 Mw 8.6 Sumatra earthquake: evidence of westward sequential seismic ruptures associated to the reactivation of a N-S ocean fabric. *Geophys. Res. Lett.* **39**, L00B07, http://dx.doi.org/10.1029/2012GL052387 (2012).
15. Hwang, L. J. & Kanamori, H. Rupture process of the 1987–1988 Gulf of Alaska earthquake sequence. *J. Geophys. Res.* **97,** 19881–19908 (1992).
16. Yue, H., Lay, T. & Koper, K. D. *En échelon* and orthogonal fault ruptures of the 11 April 2012 great intraplate earthquakes. *Nature* http://dx.doi.org/10.1038/nature11492 (this issue).
17. Meng, L. *et al.* Earthquake in a maze: compressional rupture branching during the 2012 M_w 8.6 Sumatra earthquake. *Science* **337,** 724–726 (2012).
18. Royer, J. Y., Gordon, R. G., DeMets, C. & Vogt, P. R. New limits on the motion between India and Australia since Chron 5 (11 Ma) and implications for lithospheric deformation in the equatorial Indian Ocean. *Geophys. J. Int.* **129,** 41–74 (1997).
19. Bull, J. M. & Scrutton, R. A. Fault reactivation in the central Indian Ocean and the rheology of oceanic lithosphere. *Nature* **344,** 855–858 (1990).
20. Chamot-Rooke, N. *et al.* Intraplate shortening in the central Indian Ocean determined from a 2100-km-long north-south deep seismic reflection profile. *Geology* **21,** 1043–1046 (1993).
21. Delescluse, M., Montési, L. G. J. & Chamot-Rooke, N. Fault reactivation and selective abandonment in the oceanic lithosphere. *Geophys. Res. Lett.* **35,** L16312, http://dx.doi.org/10.1029/2008GL035066 (2008).
22. Haines, A. J. & Holt, W. E. A procedure for obtaining the complete horizontal motions within zones of distributed deformation from the inversion of strain rate data. *J. Geophys. Res.* **98,** 12057–12082 (1993).
23. Cattin, R. *et al.* Stress change and effective friction coefficient along the Sumatra-Andaman-Sagaing fault system after the 26 December 2004 (Mw=9.2) and the 28 March 2005 (Mw=8.7) earthquakes. *Geochem. Geophys. Geosyst.* **10,** Q03011, http://dx.doi.org/10.1029/2008GC002167 (2009).
24. Rhie, J., Dreger, D., Bürgmann, R. & Romanowicz, B. Slip of the 2004 Sumatra-Andaman earthquake from joint inversion of long-period global seismic waveforms and GPS static offsets. *Bull. Seismol. Soc. Am.* **97,** S115–S127 (2007).

25. Ji, C. Preliminary result of the March 28, 2005 Mw 8.68 Nias earthquake. http://www.geol.ucsb.edu/faculty/ji/big_earthquakes/2005/03/smooth/nias.html (2005).
26. Vigny, C. *et al.* Insight into the 2004 Sumatra-Andaman earthquake from GPS measurements in southeast Asia. *Nature* **436,** 201–206 (2005).
27. Chlieh, M. *et al.* Coseismic slip and afterslip of the great Mw 9.15 Sumatra-Andaman earthquake of 2004. *Bull. Seismol. Soc. Am.* **97,** S152–S173 (2007).
28. Briggs, R. *et al.* Deformation and slip along the Sunda megathrust in the great 2005 Nias-Simeulue earthquake. *Science* **311,** 1897–1901 (2006).
29. Banerjee, P., Pollitz, F., Nagarajan, B. & Bürgmann, R. Coseismic slip distributions of the 26 December 2004 Sumatra-Andaman and 28 March 2005 Nias earthquakes from GPS static offsets. *Bull. Seismol. Soc. Am.* **97,** S86–S102 (2007).
30. Fujiwara, T. *et al.* The 2011 Tohoku-Oki earthquake: displacement reaching the trench axis. *Science* **334,** 1240 (2011).
31. Vigny, C. *et al.* The 2010 Mw 8.8 Maule megathrust earthquake of Central Chile, monitored by GPS. *Science* **332,** 1417–1421 (2011).
32. Fleitout, L. *et al.* Far away motions associated with giant subduction earthquakes and the mechanical properties of the lithosphere-asthenosphere system. *Geophys. Res. Abs.*, **14,** EGU2012–10899 (2012 EGU General Assembly, 2012).
33. DeMets, C., Gordon, R. G. & Argus, D. F. Geologically current plate motions. *Geophys. J. Int.* **181,** 1–80 (2010).

Supplementary Information is available in the online version of the paper.

Acknowledgements Epicentres of intraplate earthquakes were obtained from the National Earthquake Information Center (NEIC) catalogue. Focal mechanisms were obtained from the Global Centroid-Moment-Tensor (CMT) Project. Figures were prepared with GMT software. We thank R. Abercrombie for comments.

Author Contributions M.D. and N.C.-R. wrote the manuscript and prepared most of the figures with contributions from all co-authors. R.C. wrote the Coulomb stress code, L.F. and O.T. prepared the post-seismic relaxation figures and texts. C.V. has been measuring GPS velocities in southeast Asia for years, some of them being used in the kinematic model.

Author Information Reprints and permissions information is available at www.nature.com/reprints. The authors declare no competing financial interests. Readers are welcome to comment on the online version of the paper. Correspondence and requests for materials should be addressed to M.D. (delescluse@geologie.ens.fr).

METHODS

Intraplate kinematics using the Haines and Holt method. The Haines and Holt[22] method derives continuous velocity and strain-rate fields by interpolating modelled velocities that are fitted in a least-squares sense to GPS velocities. A $3^\circ \times 3^\circ$ grid was defined to cover the entire India-Australia plate. The cells located within the rigid Australia plate were not allowed to deform, as opposed to the equatorial Indian Ocean and the Indian continent. Cells are allowed to deform through an anisotropic strain-rate variance. Focal mechanisms are used to define the anisotropic variance so that the direction of the strain-rate field is controlled by the principal axis of deformations from observed seismic moment tensors. Notice that only the directions are used, as the magnitude and sign of strain-rate along the principal axis are not an input to the model. The general level of variance in cells is also a proxy for the rheology of the lithosphere. Non-uniform variance allows localization of deformation where the variance is high. In our model, heat flow is used as the proxy for the rheology of the lithosphere. As a result, cells including high heat-flow measurements are allowed to deform more. Details of the model and the earthquake catalogue can be found elsewhere[8].

Coulomb stress change calculations. We describe the two rupture zones of the 2004 and 2005 megathrust events by surfaces of displacement discontinuities in isotropic homogeneous elastic half-space. Details of the properties of slip distributions can be found elsewhere[24,25,34]. Each dislocation induces a three-dimensional stress change field, which is calculated from the analytical solution of ref. 35 using a Poisson ratio $\nu = 0.25$ and a Young's modulus $E = 75$ GPa. The Coulomb stress change is calculated on specified oriented vertical planes. To study the effect of the considered nodal planes, we assume two different receiver-fault orientations: N15°E and N110°E.

The effective friction coefficient μ' depends on the friction coefficient μ and pore-fluid migration properties related to the Skempton coefficient B on the failure plane[36]. Laboratory experiments typically find values for μ of around 0.6 to 0.85 for most rock material, apart from those rich in clay minerals[37]. The Skempton coefficient is a less well-known parameter ranging between 0.4 and 0.9 for granite, sandstone and marble[38], but still unconstrained for other rocks. Values of μ' between 0 and 0.75 are commonly assumed[39]. When μ' is high, the pore pressure does not strongly affect the normal stress. At the other extreme, when $\mu' = 0$, the rock is so saturated that the pore pressure annihilates the effect of the normal stress on the plane. Following the commonly used values[39,40] and our previous studies[23], here we assume an effective friction coefficient of 0.4.

The threshold for a Coulomb stress increase that affects seismicity is still a matter of debate. Some studies[41,42] propose a threshold of 0.01 MPa. Here colour scales are saturated for a Coulomb stress change of 0.1 MPa

Post-seismic relaxation. A two-dimensional finite element model featuring variable rheological parameters is used (Z-set/Zébulon[43]). The model considers not a single earthquake but a seismic cycle with repeating periodic earthquakes[44], with a period chosen equal to 170 yr.

An earthquake is modelled as a 10-m sudden displacement over the subduction interface. The thickness of the elastic lithosphere is chosen equal to 50 km. This value is intermediate between the thermal thickness and the flexural elastic thickness, appropriate for mimicking the lithosphere response for long timescales and large stress perturbations[45]. The asthenosphere extends between depths of 50 and 170 km. The asthenosphere deforms either as a Maxwell viscoelastic solid with a viscosity of 3×10^{18} Pa s or as a Burgers body (Kelvin-Voigt with viscosity $\eta = 3 \times 10^{18}$ Pa s, transient shear modulus $\mu = \mu_{elas}/3$, and long-term viscosity 3×10^{19} Pa s). The Kelvin-Voigt viscosity is used to model the short-term viscous response of the asthenosphere. The mantle below the asthenosphere has a viscosity of 10^{21} Pa s (of little impact on our results). Supplementary Fig. 3 only presents the central part of the finite element mesh. The computation is performed for a domain that extends horizontally from −4,000 to +4,000 km from the trench and from the Earth's surface to 1,500 km depth.

34. Ji, C., Wald, D. J. & Helmberger, D. V. Source description of the 1999 Hector Mine, California earthquake; part I: wavelet domain inversion theory and resolution analysis. *Bull. Seismol. Soc. Am.* **92,** 1192–1207 (2002).
35. Okada, Y. Internal deformation due to shear and tensile faults in a half space. *Bull. Seismol. Soc. Am.* **82,** 1018–1040 (1992).
36. Cocco, M. & Rice, J. Pore pressure and poroelasticity effects in Coulomb stress analysis of earthquake interactions. *J. Geophys. Res.* **107,** 2030, http://dx.doi.org/10.1029/2000JB000138 (2002).
37. Byerlee, J. Friction of rocks. *Pure Appl. Geophys.* **116,** 615–626 (1978).
38. Roeloffs, E. Poroelastic techniques in the study of earthquake-related hydrologic phenomena. *Adv. Geophys.* **37,** 135–195 (1996).
39. King, G., Stein, R. & Lin, J. Static stress changes and the triggering of earthquake. *Bull. Seismol. Soc. Am.* **84,** 935–953 (1994).
40. Pollitz, F., Banerjee, P., Bürgmann, R., Hashimoto, M. & Choosakul, N. Stress change along the Sunda trench following the 26 December 2004 Sumatra-Andaman and 28 March 2005 Nias earthquakes. *Geophys. Res. Lett.* **33,** L06309, http://dx.doi.org/10.1029/2005GL024558 (2006).
41. Reasenberg, P. & Simpson, R. Response of regional seismicity to the static stress change produced by the Loma Prieta earthquake. *Science* **255,** 1687–1690 (1992).
42. Stein, R. The role of stress transfer in earthquake occurrence. *Nature* **402,** 605–609 (1999).
43. Z-set. Z-set: material and structure analysis suite. http://www.zset-software.com/ (2011).
44. Thatcher, W. & Rundle, J. B. A viscoelastic coupling model for the cyclic deformation due to periodically repeated earthquakes at subduction zones. *J. Geophys. Res.* **89,** 7631–7640 (1984).
45. Watts, A. B., Bodine, J. H. & Steckler, M. S. Observation of flexure and the state of stress in the oceanic lithosphere. *J. Geophys. Res.* **85,** 6369–6376 (1980).